A host-directed adjuvant resuscitates and sensitizes intracellular bacterial persisters to antibiotics

Kuan-Yi Lu[1], Xiangbo Yang[2], Matthew J.G. Eldridge[3], Nikki J. Wagner[1], Brian Hardy[2], Matthew Axtman[2], Sarah E. Rowe[1], Xiaodong Wang[2], Sophie Helaine[3], Kenneth H. Pearce[2], Vance G. Fowler Jr[4] and Brian P. Conlon[1,5,*]

[1]Department of Microbiology and Immunology, University of North Carolina at Chapel Hill, Chapel Hill, North Carolina, USA

[2]Center for Integrative Chemical Biology and Drug Discovery, Division of Chemical Biology and Medicinal Chemistry, University of North Carolina at Chapel Hill, Chapel Hill, North Carolina, USA

[3]Department of Microbiology, Harvard Medical School, Boston, Massachusetts, USA

[4]Division of Infectious Diseases, Duke University School of Medicine, Durham, North Carolina, USA

[5]Marsico Lung Institute, University of North Carolina at Chapel Hill, Chapel Hill, North Carolina, USA

*corresponding author: brian_conlon@med.unc.edu

Keywords: Antibiotic tolerance, MRSA, Intracellular persister, Adjuvant screen, Bacterial metabolism activation

Abstract

There are two major problems in the field of antimicrobial chemotherapy–antibiotic resistance and antibiotic tolerance. In the case of antibiotic tolerance, antibiotics fail to kill the bacteria as their phenotypic state affords them protection from the bactericidal activity of the antibiotic. Antibiotic tolerance can affect an entire bacterial population, or a subset of cells known as persister cells. Interaction with the host induces the formation of persister cells in numerous pathogens, with reactive oxygen and nitrogen species production being heavily implicated in the collapse of bacterial energy levels and entrance into an antibiotic tolerant state. Here, we developed a high-throughput screen to identify energy modulators for intracellular *S. aureus*. The identified compound, **KL1**, increases intracellular bacterial energy and sensitizes the persister population to antibiotics, without causing cytotoxicity or bacterial outgrowth when used alone. We demonstrate that **KL1** exhibits adjuvant activity in a murine model of *S. aureus* bacteremia and intracellular infection of *Salmonella Typhimurium*. Further studies on its mechanism of action reveal that **KL1** suppresses the production of reactive species in host macrophages, alleviating one of the major stressors that induce antibiotic tolerance. Our findings highlight the potential to target intracellular persister cells by leveraging energy stimulators and encourage larger efforts to address antibiotic tolerance at the host–pathogen interface, particularly within the intracellular milieu.

Introduction

Antibiotic tolerance has been frequently connected with poor treatment outcomes in the clinic (1-3). Unlike antibiotic resistance, which permits bacterial growth in the presence of drugs, antibiotic tolerance allows bacteria to withstand multiple antibiotics for prolonged

47 periods (4, 5). This phenomenon is best illustrated by clinical observations in which
48 bacterial isolates that fail to respond to treatment in patients remain susceptible to the
49 prescribed antibiotics by standard minimum inhibitory concentration (MIC) testing (6, 7).
50 The extended survival of tolerant bacteria further predisposes them to evolve antibiotic
51 resistance over time, underscoring the critical need to address antibiotic tolerance (8, 9).
52
53 A principal characteristic of tolerant bacteria is their lower energy level and metabolic
54 activities, rendering a non-growing state which prevents them from being targeted by
55 antibiotics that are directed at growth-centered processes (3, 10-12). Antibiotic tolerance
56 can be induced by the infection environment and the activities of innate immune cells.
57 The intracellular environment in macrophages has been strongly associated with the
58 induction of metabolic indolence and antibiotic tolerance (13-17). Importantly, host-
59 produced reactive oxygen and nitrogen species are responsible for the induction of
60 antibiotic tolerance in a wide range of bacterial species, including *Staphylococcus aureus*,
61 *Mycobacterium tuberculosis*, *Yersinia pseudotuberculosis* and *Salmonella Typhimurium*
62 (13, 14, 16-21). Additional intracellular stressors, such as phagosome acidification and
63 nutrient deprivation, can also contribute to antibiotic tolerance (16). When conditions
64 become favorable, the intracellular bacterial persisters can resume growth, leading to
65 relapsing infections. Therefore, developing innovative strategies to target intracellular
66 bacterial persisters is essential for achieving complete eradication.
67
68 To address this difficult-to-eradicate intracellular reservoir, we established a high-
69 throughput screening platform to identify potential energy modulators, aiming to sensitize
70 these bacteria to antibiotics. Here, we targeted *S. aureus* as this versatile facultative

71 intracellular pathogen is capable of surviving within various cell types (22-26) and
72 frequently causes treatment failure and recurrent infections due to antibiotic tolerance,
73 despite appropriate use of antibiotics (7, 27). Among the >4,700 drug-like compounds
74 profiled, we identified that the lead compound **KL1** can resuscitate intracellular *S. aureus*
75 and enhance antibiotic efficacy across multiple clinical isolates and laboratory strains,
76 including methicillin-resistant *S. aureus* (MRSA). We confirm that treatment with **KL1**
77 alone does not induce bacterial outgrowth and shows no detectable cytotoxicity in
78 mammalian cells. Additionally, **KL1** exhibits adjuvant activity in a murine model of *S.*
79 *aureus* bacteremia and intracellular infection of *Salmonella Typhimurium* within
80 macrophages. Using chemical and biochemical approaches, we discover that, rather than
81 directly targeting the bacteria, **KL1** consistently reduces the levels of reactive oxygen
82 and/or nitrogen species, likely through targeting the upstream regulator EHMT2/G9a.
83 Together, we demonstrate the potential to pharmacologically sensitize intracellular
84 bacteria to antibiotics by altering the host environment. Our energy modulator screening
85 platform provides a pathway to uncover host-directed therapies that synergize with
86 antibiotics and aid in the clearance of intracellular persisters.
87

88 ## Results

89 **Intracellular environment is an important niche driving antibiotic tolerant *S. aureus***
90 Antibiotic tolerance measured in test tubes is often poorly correlated with clinical
91 outcomes in patients, highlighting the importance of probing bacterial drug responses
92 within the context of host–pathogen interactions (6). Multiple lines of evidence suggest
93 that host intracellular environment serves as a privileged site of infection that antagonizes
94 antimicrobial agents for obligate and facultative intracellular bacterial pathogens,

95 including *S. aureus* (13, 15, 28-30). This phenomenon can be illustrated by testing clinical
96 isolates with varying persister frequencies in tube assays with cell-based models. We
97 found that although two *S. aureus* isolates displayed a dramatic 500-fold difference in
98 persister formation in tubes, both produced similar high-level antibiotic tolerance following
99 internalization by bone marrow-derived macrophages (BMDMs) (**Figure 1A** and **B**). Both
100 isolates produced more tolerant bacteria inside the macrophages (46–78% of the
101 intracellular bacterial population) compared to their planktonic cultures (0.03–15% of the
102 extracellular bacteria) (**Figure 1A** and **B**). These isolates had the same minimum
103 inhibitory concentrations (MICs) for rifampicin (6 to 8 ± 4 ng/mL) and other antibiotics
104 used (Supplementary table 1). This data indicates that the host interaction plays a
105 dominant role in promoting antibiotic tolerance.
106
107 As a versatile pathogen, *S. aureus* can adapt to multiple intracellular niches and colonize
108 a wide range of mammalian cells. To facilitate tracking intracellular persister cells in vivo,
109 we constructed inducible *S. aureus* fluorescent reporter strains and first demonstrated the
110 feasibility of using these reporter strains to probe intracellular *S. aureus*. We showed that
111 viable bacteria inside macrophages can be visualized using confocal microscopy and 3D
112 rendering following induction with anhydrotetracycline (aTc) (**Figure 1C**). To explore
113 whether *S. aureus* survives antibiotic treatments inside mammalian cells, C57BL/6J mice
114 were infected with the reporter strains via tail vein injections (i.v.) and treated with 10
115 mg/kg rifampicin via the intraperitoneal (i.p.) route at 1 day post-infection (dpi). Rifampicin
116 was chosen as this drug is one of the few antibiotics that can easily penetrate mammalian
117 cells (13). The kidney cells were then extracted at 2 dpi, followed by aTc treatment to
118 induce GFP expression. The induction was performed in the presence of gentamicin to

119 exclude the extracellular bacteria. Using ImageStream analysis, we observed live cells
120 harboring GFP-expressing *S. aureus* that survived rifampicin treatment (**Figure 1D**). Thus,
121 the intracellular environment not only provides a physical barrier against antimicrobial
122 agents but also promotes antibiotic tolerance during the infection. These findings reiterate
123 the need to devise a strategy for eradicating intracellular persister cells, which is
124 particularly crucial given the limited antibiotic options available against intracellular
125 bacteria.
126

127 **A high-throughput screen for energy modulators identifies a compound that**
128 **sensitizes intracellular *S. aureus* to antibiotics**

129 Professional phagocytes, including macrophages, facilitate the clearance of bacteria
130 during bloodstream infections. However, *S. aureus* can survive this hostile environment
131 after engulfment, by adopting a less metabolically active lifestyle (22). This metabolic
132 indolence at a lower energy state favors antibiotic tolerance and persister cell formation
133 as most antibiotics are directed at growth-centered processes. To address this, we
134 developed a high-throughput platform to screen compounds that resuscitate intracellular
135 *S. aureus*, with the goal of sensitizing the intracellular population to antibiotics (**Figure**
136 **2A**). Here, we utilized a bioluminescent methicillin-resistant *S. aureus* (MRSA) strain
137 JE2–lux to probe the energy state of the intracellular bacteria (31). To assess its feasibility,
138 RAW 264.7 macrophages were infected with JE2–lux, followed by antibiotic treatment. As
139 shown in **Figure 2B**, rifampicin reduced the bioluminescent signal in the infected cells,
140 while vancomycin, which does not penetrate the mammalian plasma membrane, had no
141 effect on the intracellular *S. aureus* activity. Next, we incorporated a cell viability assay
142 into the workflow to monitor drugs' cytotoxicity. We verified that the readout reflected the

143 number of live mammalian cells without being interfered by the presence of bacteria
144 (**Figure 2C**). We then evaluated the dynamic range of the assay by measuring
145 bioluminescent signals as a function of rifampicin concentrations. The dose response
146 analysis indicated that a concentration of 2 ng/mL rifampicin resulted in a 50% reduction
147 in the intracellular bacterial activity without compromising the host cell viability (**Figure**
148 **2D**). This EC_{50} value (2 ng/mL) aligned with the rifampicin MIC (6 ng/mL) for the strain
149 JE2–lux, indicating the utility of this platform (Supplementary table 1). In comparison,
150 vancomycin did not affect the bioluminescent signal of intracellular *S. aureus* across
151 different concentrations (**Figure 2E**).
152
153 To identify energy modulators of intracellular *S. aureus* as antibiotic adjuvants,
154 macrophages infected with JE2–lux were harvested from media containing gentamicin to
155 eliminate extracellular bacteria, and then dispensed into 384-well plates with various
156 compounds (**Figure 2A**). Automatic compound dispensing was performed using a high-
157 throughput mosquito LV liquid dispenser. The bioluminescent signals and host cell
158 viability were measured immediately following a 4-hour incubation. A total of >4,700
159 compounds that share structural similarity to kinase inhibitors and comply with the
160 Lipinski's rule of five were screened (Supplementary figure 1). From this kinase-targeted
161 library, 77 compounds significantly reduced the bioluminescent signal to a level lower than
162 that of the rifampicin-treated control (three standard deviations (SD) below the control).
163 This signal reduction may indicate a decreased bacterial burden or a lower energy state
164 of the intracellular bacteria. In this screen, we did not observe any changes in persister
165 frequencies among 32 of the 77 compounds (42%) that exhibited the lowest signals.
166 Intriguingly, we identified 45 compounds that increased the bioluminescent signal by more

167 than 1.5-fold, with no detectable cytotoxicity (**Figure 3A**). We found that the top candidate
168 hit **KL1** (PubChem CID: 2881454) consistently increased the bioluminescent signal of
169 intracellular *S. aureus* (Supplementary figure 2A). This elevated signal was not a result of
170 gentamicin-killed extracellular bacteria, the host macrophages, or the compound itself
171 (Supplementary figure 2). Importantly, co-administration of **KL1** sensitized intracellular
172 MRSA to antibiotics that penetrate the mammalian plasma membrane, including
173 rifampicin and moxifloxacin, by up to 10-fold (**Figure 3B**). Treatment with **KL1** alone did
174 not induce any bacterial outgrowth, underscoring its ability to elevate the energy state of
175 intracellular *S. aureus*. The other 44 compounds did not exhibit the same adjuvant activity
176 at 10 μM, suggesting the minimum energy threshold for sensitization. To ensure its
177 reliability, we repeated the experiments using **KL1** purchased from two independent
178 suppliers and one synthesized in-house. In all cases, **KL1** increased intracellular *S.*
179 *aureus* activity and enhanced the efficacy of rifampicin in killing the intracellular bacteria
180 (Supplementary figure 3). This enhanced killing was observed across multiple laboratory
181 strains and clinical isolates, and it was proportional to **KL1**'s concentration (**Figure 3C–D**
182 and Supplementary figure 4). Furthermore, **KL1** retained its ability to synergize with
183 rifampicin even when the intracellular bacteria were pretreated with the antibiotic,
184 suggesting that low-energy persisters may be resuscitated and sensitized to antibiotic
185 treatment (**Figure 3E**). Together, we demonstrated the feasibility of pharmaceutically
186 sensitizing the intracellular *S. aureus* persisters to antibiotics and confirmed that
187 screening these sensitizers using our newly established semi-automated high-throughput
188 platform is viable.
189
190 **Compound KL1 exhibits adjuvant activity in a mouse model for *S. aureus* sepsis**

191 **and a cell-based *Salmonella* infection model**

192 Next, we evaluated the in vivo efficacy of **KL1** using our *S. aureus* bacteremia model (13).
193 Briefly, C57BL/6J mice were intravenously injected with *S. aureus* to induce a systemic
194 infection. At 6 hours post-infection (hpi), mice were administered 10 mg/kg rifampicin once
195 daily (q.d.), either alone or in combination with 100 mg/kg **KL1** twice daily (b.i.d.), via
196 intraperitoneal injections (**Figure 4A**). After a 48-hour treatment regimen, the livers and
197 spleens were harvested, and the tissue homogenates were plated to determine the
198 number of bacteria that survived the antibiotic treatment. Our data showed that combined
199 administration of **KL1** and rifampicin further reduced the bacterial burden in both the liver
200 and spleen, compared to rifampicin alone (**Figure 4B** and **C**). This animal experiment was
201 replicated on separate days using both male and female mice from different litters, which
202 each group consisting of 6–8 mice, to ensure reproducibility.

203

204 Since **KL1** may or may not directly target the bacteria and may instead modulate host–
205 pathogen interactions, we explored the possibility that **KL1** might also affect other
206 intracellular bacteria. Here, we opted to investigate the gram-negative bacterium
207 *Salmonella typhimurium* because it also survives within macrophages and forms
208 antibiotic-tolerant persister cells (16). Strikingly, **KL1** exhibited adjuvant activity when
209 combined with ciprofloxacin and enhanced the killing of *Salmonella typhimurium* in
210 macrophages (**Figure 4D**). This data suggests that **KL1** may serve as a potential broad-
211 acting antibiotic adjuvant against intracellular bacteria.

212

213 **KL1 does not directly act on *S. aureus***

214 Since the **KL1**-mediated synergy was likely energy-dependent, we utilized a mutant

215 MRSA strain lacking all four glucose transporters (ΔG4) to test if the bacterial central
216 metabolism was crucial for **KL1**'s activity (32). We found that the adjuvant activity of **KL1**
217 against intracellular *S. aureus* was substantially attenuated in the absence of functional
218 glucose uptake (Supplementary figure 5). This finding aligned with the hypothesis that
219 **KL1** enhanced antibiotic efficacy by modulating the energy state of intracellular bacteria
220 and suggested that glucose utilization was essential for sensitization of the tolerant cells.
221
222 To deconvolute **KL1**'s mechanism of action, we interrogated whether **KL1** impacted
223 extracellular *S. aureus* in planktonic cultures. We began by testing **KL1**'s activity in
224 actively growing *S. aureus* at the mid-exponential phase (high energy state). In this case,
225 no increase in energy was detected with 10 μM **KL1**, despite observing a moderate
226 increase at the higher concentration of 40 μM (Supplementary figure 6A). Treatment with
227 **KL1** at the higher concentration did not alter bacterial growth, nor did it affect persister
228 frequency following rifampicin treatment (Supplementary figure 6B). Similarly, **KL1** did not
229 affect the energy state or growth pattern of non-growing, stationary-phase bacteria (low
230 energy state) in the presence or absence of antibiotics (Supplementary figure 6C and D).
231
232 We subsequently employed Seahorse analysis to investigate whether **KL1** altered the
233 metabolic activity of extracellular *S. aureus*. This analysis measures real-time changes in
234 cellular metabolism and has been applied to investigate bacterial respiration in *S. aureus*
235 (33). Our data clearly showed that **KL1** had no effect on the oxygen consumption rate
236 (OCR) and extracellular acidification rate (ECAR) of *S. aureus* in planktonic cultures
237 (Supplementary figure 7A and B). Additionally, we directly measured the relative ATP
238 levels in the bacteria and did not observe any changes across multiple *S. aureus* strains

239 (Supplementary figure 7C–E). Collectively, our data strongly suggested that **KL1** did not
240 directly target the bacteria but may perturb the host–pathogen interaction by altering the
241 intracellular environment.
242
243 **KL1 modulates the host cells and reduces the level of reactive species**
244 Thus far, the mode of action of **KL1** has not been reported, but this compound has been
245 included in hundreds of biological screens. Among these screens, **KL1** was found to be
246 active in five bioassays targeting four different proteins (Supplementary table 2).
247 EHMT2/G9a, in particularly, stood out as a potential candidate target of **KL1** given that
248 this epigenetic regulator is an intracellular protein expressed in immune cells, including
249 macrophages. Additionally, the EC_{50} values of KL1 (25 μM) determined in the previous
250 EHMT2/G9a inhibition assay (PubChem AID: 504332) aligned with the adjuvant activity
251 of **KL1** (10–40 μM) identified in this study. To interrogate EHMT2/G9a as a potential target,
252 we first utilized the highly selective EHMT inhibitor BIX-01294 to assess whether
253 EHMT2/G9a influences antibiotic susceptibility of intracellular *S. aureus*. Surprisingly, we
254 found that inhibition of EHMT2/G9a also elevated the energy state of intracellular *S.*
255 *aureus* and synergized with rifampicin in a dose-dependent manner, similar to the effect
256 observed with the identified compound **KL1** (**Figure 5A** and **B**). Intriguingly, EHMT2/G9a
257 plays a key role in the intracellular innate immunity and modulates macrophage
258 polarization in response to microbial infections (34-36). In this context, a critical
259 downstream function mediated by EHMT2/G9a is the production of reactive oxygen and
260 nitrogen species (ROS/RNS). We have previously shown that ROS and host-derived
261 peroxynitrite can induce antibiotic tolerance in intracellular *S. aureus*, and ROS/RNS have
262 been implicated in the induction of antibiotic tolerance and persister cells in various

263 bacterial species (13, 14, 16-19, 37). Thus, we hypothesized that **KL1** targets
264 EHMT2/G9a and alleviates the production of ROS/RNS, which in turn facilitates the
265 antibiotic killing of intracellular bacteria. To test this hypothesis, we employed two probing
266 methods with distinct detection mechanisms to measure reactive species. Specifically, a
267 chemiluminescent probe L-012 and a fluorescent probe fluorescein-boronate (Fl-B) were
268 applied. Using both methods, we consistently observed that **KL1** at 40 and 100 μM
269 significantly reduced the levels of ROS/RNS in *S. aureus*-infected macrophages at 4- and
270 8-hours post-treatment (**Figure 5C–D** and Supplementary figure 8). Notably, treatment
271 with the EHMT2/G9a inhibitor BIX-01294 and the antioxidant control butylated
272 hydroxyanisole (BHA) both resulted in a similar decrease in ROS/RNS. Furthermore, **KL1**
273 was able to lessen the levels of ROS/RNS in uninfected macrophages (Supplementary
274 figure 8B and D). Altogether, these results support the hypothesis that **KL1** enhances
275 antibiotic killing of intracellular bacteria by reducing oxidative stress in the intracellular
276 milieu, presumably by targeting the epigenetic regulator EHMT2/G9a (**Figure 6**).
277

278 ## Discussion

279 The ability of bacterial pathogens to survive high concentrations of bactericidal antibiotics
280 for extended periods, despite lacking resistance mutations, is likely a major factor
281 contributing to treatment failure. Patients with *S. aureus* bacteremia receiving appropriate
282 antibiotic therapy for at least 2–6 weeks remain at a 20–30% risk of treatment failure (38-
283 40). The weak correlation between the in vitro antimicrobial susceptibility testing results
284 and clinical outcomes highlights the importance of considering the relevant physiological
285 context when addressing the poor antibiotic efficacy in clinical settings (6).
286

287 Devising novel strategies against bacterial persister cells has drawn increasing attention
288 over the years (41-43). Conceptually, the eradication of persister cells can be achieved
289 either by directly targeting the persister cells or by reverting them to a metabolically active
290 state, thereby making them vulnerable to antibiotics. The intracellular environment is a
291 well-established reservoir for antibiotic tolerant persister cells. In this study, we
292 demonstrate the potential of altering the host microenvironment to sensitize intracellular
293 persisters to antibiotics and improve treatment outcomes. Although different stress stimuli
294 can lead to the formation of antibiotic tolerant persister cells, all result in the production
295 of a metabolically indolent population that can withstand antibiotic challenge. We
296 therefore employed the bioluminescent reporter to probe the energy levels of intracellular
297 bacteria as part of a phenotypic screen. Given that the low-energy, low-metabolic activity
298 state is central to antibiotic tolerance and persistence, the developed screening platform
299 offers broader applications and may be adapted for other intracellular pathogens across
300 various host cell types and will be agnostic to the mechanism responsible for the induction
301 of antibiotic tolerance (44-47).
302
303 Intriguingly, our lead compound **KL1** significantly reduced ROS/RNS production in
304 macrophages, sensitized intracellular *S. aureus* and *Salmonella* persister cells to
305 antibiotic treatment, and enhanced antibiotic efficacy in a murine infection model. These
306 findings strongly support that: 1) Targeting host pathways can render intracellular
307 persisters more susceptible to antibiotics; 2) ROS/RNS are key drivers of antibiotic
308 tolerance in vivo; 3) Inhibiting ROS/RNS production can sensitize persister cells across
309 diverse bacterial species; and 4) Sensitizing intracellular persisters leads to improved
310 antibiotic efficacy against active infections. This work underscores the potential of using

311 host-directed therapeutics, in conjunction with antibiotics, to enhance treatment outcomes.
312 Continued development of our screening platform promises identification of additional
313 host-targeted drugs that sensitize intracellular persisters to antibiotics. Ongoing studies
314 on **KL1**'s mechanism of action, along with medicinal chemistry optimization and in vivo
315 testing in combination with various antibiotics against multiple pathogens, including *M.*
316 *tuberculosis*, will be critical in determining the full therapeutic potential of this host-
317 directed adjuvant in eradicating deep-seated infections.
318

319 ## Materials and methods

320 ### General materials

321 Antibiotics including rifampicin (Rif), moxifloxacin hydrochloride (Mox), gentamicin sulfate
322 (Gen) were purchased from Fisher Scientific with >95% purity. Vancomycin hydrochloride
323 (Van) (>99% purity) was purchased from Alfa Aesar. Compound **KL1** was obtained from
324 multiple sources (ChemBridge Corporation, Enamine and synthesized in-house
325 (Supplementary Information)) with >90% purity to validate the fidelity of this compound.
326 The G9a inhibitor, BIX-01294 (>98% purity), was purchased from MedChemExpress.
327 RAW 264.7 macrophages were obtained from ATCC (TIB-71) and distributed by the
328 Tissue Culture Facility at the University of North Carolina at Chapel Hill. RAW 264.7 cells
329 were maintained in complete DMEM (Dulbecco's Modified Eagle Medium (Gibco)
330 supplemented with 10% (vol/vol) heat-inactivated fetal bovine serum (FBS) (Avantor
331 Seradigm, premium grade), 2 mM L-glutamine (Gibco), 1x non-essential amino acids
332 solution (Gibco) and 1 mM sodium pyruvate (Gibco)) below 18 passages without reaching
333 more than 90% confluency. Bone marrow-derived macrophages (BMDMs) were isolated
334 from C57BL/6J mice (The Jackson Laboratory; strain number 000664) and cultivated in

335 complete DMEM as previously described (48). Immortalized BMDMs were generated
336 using a CRE-J2 retroviral infection method (49). Briefly, C57BL/6J mouse-derived
337 BMDMs were cultured in 50% (vol/vol) L929 fibroblast-conditioned medium and infected
338 with CRE-J2 retrovirus on day 5 and day 7. Transduced cells were continuously cultured
339 in the conditioned medium, with the concentration gradually reduced to 20% conditioned
340 medium. The immortalized BMDMs were maintained in RPMI 1640 (Corning)
341 supplemented with 2 mM L-glutamine, 1x Penicillin-Streptomycin (GenClone), 10%
342 (vol/vol) heat-inactivated FBS (R&D Systems) and 20% conditioned medium.
343

344 **Bacterial strains and growth conditions**

345 *S. aureus* strains LAC (USA300), HG003, JE2 (USA300), JE2–lux (JE2*lux*ABDCE)
346 (kindly provided by Roger Plaut, Center for Biologics Evaluation and Research, Silver
347 Spring, United States) (31), ΔG4 (kindly provided by Anthony Richardson, University of
348 Pittsburgh, Pittsburgh, United States) (32) and the *S. aureus* bacteremia isolates (14)
349 were routinely cultured in tryptic soy broth (TSB) (Fisher Scientific) at 37 °C and 225 rpm
350 unless otherwise stated. The clinical isolates were obtained under an IRB exemption from
351 a preexisting collection. *Salmonella enterica serovar Typhimurium* strain 14028S was
352 cultured in LB broth (Lennox) at 37 °C with shaking.
353

354 **Minimum inhibitory concentration assay**

355 Stationary-phase bacterial cultures were diluted at 1:1,000 in Mueller–Hinton broth (MHB)
356 (Oxoid) containing serially diluted Rif (0–0.2 μg/mL), Mox (0–20 μg/mL) or Van (0–16
357 μg/mL) in 96-well assay plates (Corning) in triplicates (200 μL/well). Plates were sealed
358 with Breathe-EASIER membranes (Diversified Biotech) and incubated statically at 37 °C

359 for 24 h. The minimum inhibitory concentrations (MICs) were determined by the absence
360 of bacterial growth. Three independent assays were performed to ensure the
361 reproducibility.
362
363 **Construction of the inducible reporter strains**
364 The plasmid pALC2084 containing a tetracycline (Tet)-inducible GFP-expressing cassette
365 (50) (kindly provided by Ambrose Cheung, Dartmouth College, Hanover, United States)
366 was transformed into a *S. aureus* intermediate strain RN4220 using a Gene Pulser Xcell
367 electroporation system (Bio-Rad) as previously described (51). The plasmid was
368 subsequently purified and transformed into the recipient *S. aureus* strain HG003. Single
369 colonies were isolated and cultured in TSB containing 10 μg/mL Cam and 0–2 μM
370 anhydrotetracycline hydrochloride (aTc) (Sigma) for 2–3 h. The induction of GFP
371 expression was verified at an excitation and emission wavelength of 475 nm and 508 nm
372 using a Synergy H1 microplate reader (BioTek). To construct the mKate reporter plasmid,
373 the DNA fragment of mKate2 was amplified from pRN10 (Addgene plasmid: 84454) (52)
374 using a specific primer pair (Supplementary information) and Q5 High-Fidelity DNA
375 Polymerase (New England Biolabs). The PCR product was purified using a MinElute
376 Reaction Cleanup kit (Qiagen). A Tet-inducible expression vector pRMC2 (Addgene
377 plasmid: 68940) (53) and the mKate DNA fragments were subjected to KpnI-HF and
378 EcoRI-HF (New England Biolabs) enzymatic digestion and agarose gel electrophoresis.
379 The DNA fragments were gel purified using a QIAquick PCR purification kit (Qiagen) and
380 underwent ligation with T4 DNA ligase (New England Biolabs) at 16 °C for 16 h. The
381 ligation product was transformed into MAX Efficiency DH5α competent cells
382 (ThermoFisher Scientific) according to the manufacturer's instruction. Site-directed

383 mutagenesis was performed using a QuikChange kit (Agilent Technologies) and a primer
384 pair (Supplementary information) to incorporate an upstream ribosomal binding site. The
385 final pRMC2-mKate construct was verified by restriction digest mapping and Sanger
386 sequencing. The plasmid pRMC2-mKate was transformed into strain RN4220, followed
387 by the recipient strain HG003 as described above. The aTc-induced mKate expression
388 was confirmed by measuring at 633 nm with excitation at 588 nm using a Synergy H1
389 microplate reader.
390
391 **Antibiotic survival assays**
392 For *S. aureus* planktonic cultures, 16- to 18-h stationary cultures were diluted at 1:100 in
393 MHB and incubated at 37 °C and 225 rpm for 3 h to reach the mid-exponential phase.
394 The bacterial cultures were then treated with 10 μg/mL Rif and/or 0–40 μM **KL1** at 37 °C
395 and 225 rpm for 24 h. The bacteria were washed in one volume of sterile 1% NaCl three
396 times at 20,000 *g* for 5 min, followed by resuspending in one volume of 1% NaCl. The
397 bacterial suspensions were 10-fold serially diluted and plated on tryptic soy agar (TSA)
398 to enumerate the number of survivor *S. aureus*. The frequencies of tolerant bacteria were
399 calculated by normalizing the numbers of survivor bacteria to the numbers of input
400 bacteria (T_0).
401
402 To assess the intracellular *S. aureus* persister frequencies, RAW 264.7 macrophages or
403 BMDMs were seeded in Costar 24-well tissue culture-treated plates (Corning) (500 μL of
404 $4x10^5$ cells per well) in complete MEM (Minimum Essential Medium (Gibco)
405 supplemented with 10% (vol/vol) heat-inactivated fetal bovine serum and 2 mM L-
406 glutamine) at 37 °C and 5% CO_2 for 16 h. Macrophages were infected with *S. aureus*

407 strains at a multiplicity of infection (MOI) of 10 by centrifugation at 1,000 *g* for 2 min,
408 followed by incubation at 37 °C for 35 min. After removal of the spent medium, infected
409 cells were incubated in 500 μL complete MEM containing antibiotics (10 μg/mL Rif, 50
410 μg/mL Mox or 20 μg/mL Van) in the presence or absence of 0–40 μM **KL1** or 0–10 μM
411 BIX-01294 in the presence of 50 μg/mL Gen at 37 °C and 5% CO_2 for 24 h. The cells
412 were washed three times in 1 mL PBS and lysed with 200 μL 0.5% (vol/vol) Triton X-100
413 (Fisher Scientific) at 37 °C for 5 min, followed by the addition of 800 μL PBS. The released
414 intracellular *S. aureus* were 10-fold serially diluted and plated on TSA for enumeration.
415 For the persister frequencies, the numbers of survivor bacteria were normalized to the
416 corresponding numbers of intracellular bacteria before the antibiotic treatment (T_0). For
417 comparison between different treatment groups, the intracellular *S. aureus* loads were
418 normalized against the untreated controls at the endpoint (24-h post-treatment).
419
420 For *Salmonella* infections, immortalized BMDMs were seeded in 12-well tissue culture-
421 treated plates ($4x10^5$ cells per well) in RPMI 1640 supplemented with 2 mM L-glutamine
422 and 10% (vol/vol) heat-inactivated FBS at 37 °C and 5% CO_2 for 24 h. The stationary-
423 phase bacteria were opsonized with 8% (vol/vol) mouse serum in the RPMI 1640 medium
424 for 20 min and applied to the immortalized BMDMs at an MOI of 15 as previously
425 described (29). The plates were centrifuged at 110 *g* for 5 min and incubated at 37 °C and
426 5% CO_2 for 30 min. Cells were washed once with PBS and incubated in RPMI 1640
427 medium containing 5 μg/mL ciprofloxacin hydrochloride (MP Biomedicals) in the presence
428 of 10–80 μM **KL1** or 0.2% DMSO at 37 °C and 5% CO_2 for 24 h. The cells were washed
429 three times in 500 μL PBS and lysed with 0.2% (vol/vol) Triton X-100 at 37 °C for 10 min.
430 The extracted intracellular *Salmonella Typhimurium* were plated on LB agar to determine

431 the number of survivor bacteria. The persister frequencies were calculated by normalizing
432 the final CFUs (T_{24}) to the input CFUs (T_0).
433
434 **Live cell microscopy**
435 RAW 264.7 macrophages were seeded in a Nunc 8-well Lab-Tek chambered coverglass
436 (ThermoFisher Scientific) (500 µL of 2–3x10^5 cells per well) in complete MEM at 37 °C
437 and 5% CO_2 for 16 h. Cells were infected with the Tet-inducible GFP- or mKate-
438 expressing *S. aureus* strains at an MOI of 20 (without Rif) or 100 (with Rif) by
439 centrifugation at 1,000 *g* for 2 min and incubating at 37 °C for 35 min. Cells were washed
440 once in 500 µL complete MEM and treated with and without 10 µg/mL Rif in the presence
441 of 50 µg/mL Gen at 37 °C for 1.5 h (without Rif) and 4 h (with Rif). Rif-treated cells were
442 washed three times with 500 µL complete MEM and incubated in the medium containing
443 50 µg/mL Gen at 37 °C for 2–3 h to allow for resuscitation of the intracellular *S. aureus*
444 persisters. Infected cells were then treated with 2 µM aTc in the presence of 50 µg/mL
445 Gen at 37 °C for 3 h to induce GFP and mKate expression. Macrophages harboring GFP-
446 expressing *S. aureus* were imaged using a Leica SP8X Falcon (Leica Microsystems) with
447 the following settings: (1) a tunable white light laser (WLL2) set to 484 nm was used for
448 excitation with fluorescence detection at 495–570 nm and a detector gain of 100 V; (2) a
449 1024 X 1024 pixel scan at 16-bit with a scanning speed set to 600 was applied; (3) the
450 pixel averaging was set to 2; (4) the pinhole size was set to 1 AU; (5) single images were
451 obtained using a 63x oil-immersion objective lens (Plan-Apochromat, NA 1.4) with an 1
452 to 4-fold zoom. Macrophages infected with mKate-expressing *S. aureus* were stained with
453 100–300 nM LysoTracker Green DND-26 (ThermoFisher Scientific) at 37 °C for 30 min.
454 The dye-loaded cells were washed once and kept in 200 µL complete MEM containing 1

455 μg/mL Hoechst 33342, 50 μg/mL Gen and 2 μM aTc. The z-stack acquisition and time-
456 lapse live imaging were carried out using an Olympus FV3000RS confocal microscope
457 (Olympus Life Science) equipped with a stage-top incubator at 37 °C, 5% CO_2 and 100%
458 humidity. The microscope settings were as follows: (1) 405-nm (Hoechst 33342), 488-nm
459 (LysoTracker Green) and 594-nm (mKate) diode lasers were used for excitation with
460 highly sensitive fluorescence spectral GaAsP detectors; (2) a 516 X 516 pixel scan was
461 applied; (3) the pixel averaging was set to 10; (4) the pinhole size was set to 1 AU; (5)
462 single images were obtained using a 60x oil-immersion objective lens (Super Correction,
463 NA 1.4). All confocal images were exported as the default with no gamma correction by
464 ImageJ/FIJI (54).
465
466 **Mouse infection and isolation of kidney cells**
467 C57BL/6J mice (6- to 9-week-old) were systemically infected with the Tet-inducible GFP-
468 expressing *S. aureus* strain HG003 ($5x10^6$ CFU) via the tail vein intravenous route (13).
469 At 1 day post-infection (dpi), mice were administered with 10 mg/kg Rif in 2.5% DMSO,
470 12.5% polyethylene glycol (PEG300) (Sigma) and 85% sterile H_2O via intraperitoneal
471 injection. Infected mice received the vehicle (2.5% DMSO/12.5% PEG300) were included
472 as a control. At 2 dpi (24-h Rif treatment), dissected mouse kidneys were homogenized
473 in 5 mL cold PBS containing deoxyribonuclease I (50 U/mL, bovine pancreas)
474 (ThermoFisher Scientific) using a Stomacher 80 Biomaster (Seward, USA) at fast speed
475 for 2 min twice (55). Tissue homogenates were filtered through 70-μm strainers (VWR
476 International) and pelleted at 300 *g* for 5 min at 4 °C. After three washes in 4 mL cold PBS
477 in 5-mL polypropylene round-bottom tubes (Corning) at 300 *g* for 5 min at 4 °C, cells were
478 resuspended in cold PBS containing 1% fetal bovine serum and 50 μg/mL Gen in the

479 presence or absence of 2 μM aTc for 3 h. The cell suspensions were probed with
480 LIVE/DEAD fixable violet dead cell stain (1 μL/1 mL) (ThermoFisher Scientific) at 4 °C for
481 30 min before ImageStream analysis.
482
483 To evaluate the adjuvant activity of **KL1** in vivo, C57BL/6J mice were infected by
484 intravenous injection with $2x10^7$ CFU of *S. aureus* strain HG003. At 6 hours post-infection
485 (hpi), mice were administered with 10 mg/kg Rif, either alone or in combination with 100
486 mg/kg **KL1** in 7% DMSO, 40% PEG300 and 53% sterile H_2O via intraperitoneal injection.
487 Rif and **KL1** were administered once a day (q.d.) and every 12 h (b.i.d.), respectively, for
488 2 days. After 48 h treatment, dissected mouse organs were homogenized either by
489 repetitively rolling a serological pipette over the samples in the sample bags (liver) or by
490 bead beating using a Precellys 24 Touch (Bertin Technologies) at 5,000 rpm for 25 s twice
491 with a 5 s interval (spleen). Tissue homogenates were 10-fold serially diluted in 1% NaCl
492 and plated on TSA for the enumeration of survivor bacteria. The bacterial burden (CFU/g)
493 was calculated by normalizing the number of CFU to the tissue weight.
494
495 **ImageStream analysis**
496 Cell suspensions were loaded into an Amnis ImageStreamX Mark II (EMD Millipore) for
497 single-cell imaging and fluorescence detection. For capturing live cells harboring viable
498 GFP-expressing *S. aureus*, 405-nm and 488-nm colinear lasers were set to 40 mW and
499 70–90 mW for the live/dead cell discrimination and GFP expression, respectively. In-focus
500 single-cell images were acquired with a 60X magnification and a low-speed flow rate
501 using the INSPIRE software (EMD Millipore). The exported data were analyzed using
502 IDEAS 6.2 software (EMD Millipore).

503

504 **High-throughput screen for intracellular *S. aureus* energy modulators**

505 RAW 264.7 macrophages were seeded in 4 mL complete MEM in Costar 6-well tissue
506 culture-treated plates (Corning) ($8x10^5$ cells/well) at 37 °C and 5% CO_2 for 16 h. Cells
507 were infected with *S. aureus* strain JE2–Lux at an MOI of 100 at 37 °C for 25 min. The
508 infected macrophages were washed once with 2 mL PBS and incubated with 10 mM
509 EDTA in PBS (2 mL/well) at 37 °C for 5–10 min. After dissociation, cells were pelleted at
510 300 *g* for 6 min, resuspended in complete MEM containing 50 µg/mL Gen at a density of
511 $2.5x10^5$ cells/mL and dispensed 80 µL of the cell suspension into each well of 384-well
512 tissue culture-treated white plates and optically clear polymer bottom black plates
513 (ThermoFisher Scientific) for luminescence and fluorescence detections, respectively.
514 Uninfected macrophages were also added to column 1 and 24 of each plates as controls
515 for the luminescence background and the baseline of host cell viability. The plates were
516 preloaded with 80 nL of 10 mM compounds using a Mosquito LV multichannel pipetting
517 system (SPT Labtech, Covina). The vehicle control (0.1% DMSO) and 10 µg/mL Rif were
518 included in each experiment for comparison. After cell dispensing, the plates were
519 centrifuged at 500 *g* for 2 min and incubated in a humidified chamber at 37 °C and 5%
520 CO_2 for 4 h. The luminescence signals were measured at an 1.25-mm depth with a
521 detector gain of 250 at 37 °C using a Synergy H1 microplate reader. To monitor the cell
522 viabilities after compound treatment, 10 µL CellTiter-Fluor reagent (Promega) were added
523 to the black plates and incubated in the dark at 37 °C and 5% CO_2 for 30 min. The
524 fluorescence intensities were measured at a 7-mm depth with a detector gain of 100 at
525 37 °C. The kinase-targeted compound library containing >4,700 rule of five-compliant
526 compounds were part of the chemical collection at the Center for Integrative Chemical

527 Biology and Drug Discovery (CICBDD) at the University of North Carolina at Chapel Hill.
528 The luminescence and fluorescence signals were normalized to the corresponding
529 vehicle controls (0.1% DMSO). EC_{50} values of Van and Rif for the intracellular MRSA
530 strain JE2–Lux were determined by fitting the luminescence data to a standard dose
531 response equation (GraphPad Prism).
532
533 **Reactive species assays**
534 The reactive oxygen and nitrogen species were measured using a luminescent probe L-
535 012 (Wako Chemical Corporation) and a fluorescent dye fluorescein-boronate (Fl-B) (48).
536 For L-012 probing, RAW 264.7 macrophages were seeded in 100 μL complete MEM in
537 Falcon 96-well tissue culture-treated white plates (Corning) (3.84×10^4 cells/well) at 37 °C
538 and 5% CO_2 for 16 h. Cells were infected with *S. aureus* strain JE2 at an MOI of 10 by
539 centrifugation at 1,000 *g* for 2 min, followed by incubation at 37 °C for 40 min. Cells were
540 treated with 40–100 μM **KL1** or 1–10 μM BIX-01294 in the presence of 50 μg/mL Gen in
541 five replicates at 37 °C and 5% CO_2 for 4–8 h. After three washes with 200 μL pre-warmed
542 PBS, 100 μL of 300 μM pre-warmed Hanks' balanced salt solution (Gibco) was added to
543 each well. The luminescence signals were immediately measured with auto-gain at 37 °C
544 using a Synergy H1 microplate reader. The signals of two consecutive reads were
545 averaged to minimize the technical variability between reads. For Fl-B staining,
546 macrophages were seeded in 96-well tissue culture-treated black clear-bottom plates
547 (Corning) with the same culture condition. After treatment with 40–100 μM **KL1**, 1–10 μM
548 BIX-01294 or 20 μM butylated hydroxyanisole (Sigma), infected cells were washed twice
549 with 200 μL pre-warmed PBS and incubated with 100 μL of 25 μM Fl-B in PBS at 37 °C
550 for 30 min. Cells were washed three times with 200 μL PBS to remove unbound dyes and

551 maintained in 100 μL PBS. The fluorescence signals were measured at 535 nm with
552 excitation at 485 nm with a detector gain of 100 and an area scan mode using a Synergy
553 H1 microplate reader.
554
555 **ATP measurement**
556 *S. aureus* strains LAC, HG003 and JE2 were grown in TSB for 16–18 h and subcultured
557 at 1:1,000 to 1:40,000 dilution in fresh TSB containing 40 μM **KL1** or 0.1–0.5% DMSO in
558 six replicates at 37 °C for 4 h. The bacterial cultures were then aliquoted into Falcon 96-
559 well white plates (100 μL/well) and mixed with one volume of BacTiter-Glo reagent
560 (Promega), followed by incubation in the dark on a rocker with gentle shaking at room
561 temperature for 20 min. The luminescence signals were detected at a 1.25-mm depth
562 with a detector gain of 250 using a Synergy H1 microplate reader and normalized to the
563 corresponding CFUs to determine the relative ATP levels.
564
565 **Seahorse analysis**
566 The stationary-phase bacterial cultures were diluted at 1:100 in fresh TSB in triplicate and
567 incubated for 2–3 h until the OD_{600} values reached 0.3. Each culture was then diluted at
568 1:500 to 1:1,000 in TSB or Seahorse XF DMEM (Agilent Technologies) supplemented
569 with 100 mM glucose, 2 mM L-glutamine and 1 mM sodium pyruvate and dispensed into
570 a poly-D-lysine (PDL)-coated Seahorse XF HS miniplate (100 μL/well). PDL-coating was
571 performed by adding 100 μg/mL PDL in sterile H_2O to each well of the miniplate for 30
572 min. Excessive PDL was removed by two washes with H_2O, and the miniplate was air-
573 dried prior to the assays. Bacteria adherence was achieved by centrifugation at 1,400 *g*
574 for 10 min. An additional 80 μL media was carefully added to each well (180 μL final

575 volume), and the miniplate was loaded into a pre-calibrated Seahorse XF HS Mini
576 Analyzer (Agilent Technologies). A final concentration of 40 μM of **KL1** or 0.1–0.5%
577 DMSO was injected into each well, and the oxygen consumption rates (OCRs) and
578 extracellular acidification rates (ECARs) of the bacteria were monitored at 37 °C for 4–6
579 h. The data was analyzed using Seahorse Analytics (Agilent Technologies) and plotted
580 using GraphPad Prism.
581
582 **Databases**
583 Biological test results of the identified compound **KL1** (PubChem CID: 2881454) were
584 retrieved from PubChem (https://pubchem.ncbi.nlm.nih.gov/) (56). Gene expression
585 profiles were examined using Expression Atlas (https://www.ebi.ac.uk/gxa/home) (57).
586 Biological functions and subcellular localization data were sourced from the UniProt
587 Knowledgebase (https://www.uniprot.org/) (58). Chemical structures were generated
588 using ChemDraw software 21.0.0 (PerkinElmer).
589
590 ## Acknowledgements
591 This work was supported by the Burroughs Wellcome Fund (BWF) in Pathogenesis of
592 Infectious Disease (PATH award to B.P.C), the National Institutes of Health (NIH)
593 (R01AI173004 and R01AI179695 to B.P.C and R01AI167978 to S.E.R) and UNC
594 Lineberger Comprehensive Cancer Center. The content of this study is solely the
595 responsibility of the authors and does not necessarily represent the official views of the
596 funding agents. We are grateful to the UNC Neuroscience Microscopy Core and the UNC
597 Flow Cytometry Core Facility (supported in part by P30 CA016086). Part of the figures
598 was created with BioRender.com.

Footnotes

To whom correspondence should be addressed. Email: brian_conlon@med.unc.edu

The authors have no competing interests.

604 **Figures**

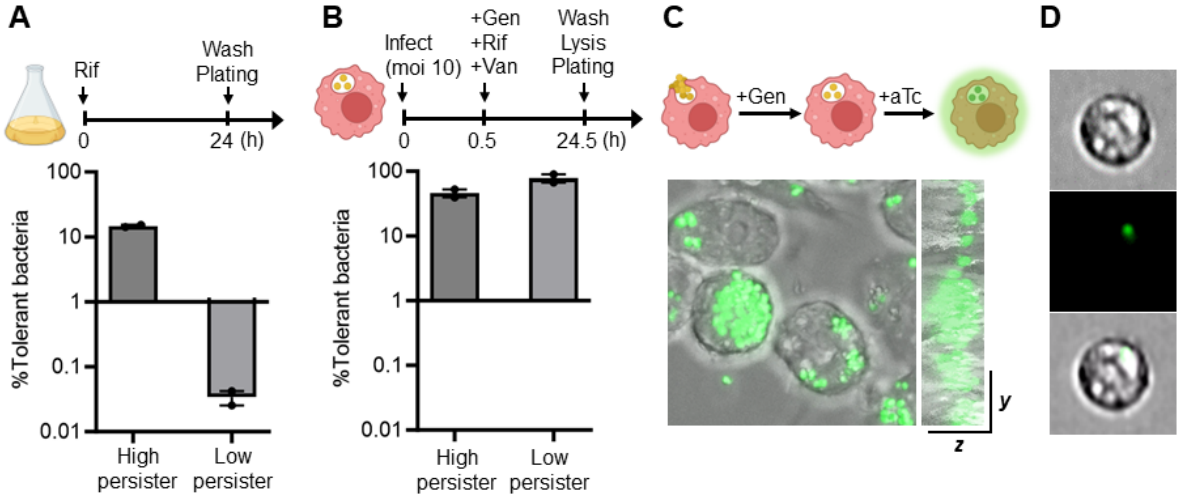

605

606 **Figure 1. Intracellular environments provide an important niche producing**
607 **antibiotic-tolerant *S. aureus* persisters.** (**A**) Clinical isolates from *S. aureus* bacteremia
608 patients exhibited variable antibiotic tolerability in planktonic cultures. Rifampicin (Rif) was
609 washed away to enumerate the numbers of survivor bacteria (CFU). (**B**) The high and low
610 persister isolates characterized in (**A**) became more tolerant and produced comparable
611 numbers of persisters in bone marrow-derived macrophages. Gentamicin (Gen) and
612 vancomycin (Van) were administered to eradicate the extracellular bacteria. The numbers
613 of survivor bacteria were normalized to the corresponding numbers of intracellular CFUs
614 before the antibiotic treatment (T_0) to calculate the persister frequencies. Representative
615 data of three independent experiments are shown (n = 3). The bars represent mean ±
616 SEM. Assay schematics are shown above plots. (**C**) Confocal z-sectioning visualized
617 viable intracellular *S. aureus*. RAW 264.7 macrophages were infected with an inducible
618 GFP reporter strain and treated with 50 μg/mL Gen to exclude extracellular *S. aureus*.
619 Live intracellular bacteria can be probed with anhydrotetracycline (aTc) induction. (**D**)
620 Intracellular persisters in mouse kidneys were detected using ImageStream analysis.

621 C57BL/6J mice were systemically infected with the inducible reporter strain via the
622 intravenous route and intraperitoneally treated with 10 mg/kg Rif at 1 day post-infection
623 (dpi) for 24 h. The kidney cells were extracted at 2 dpi and incubated with 2 μM aTc to
624 induce GFP expression. Representative images are shown.
625
626

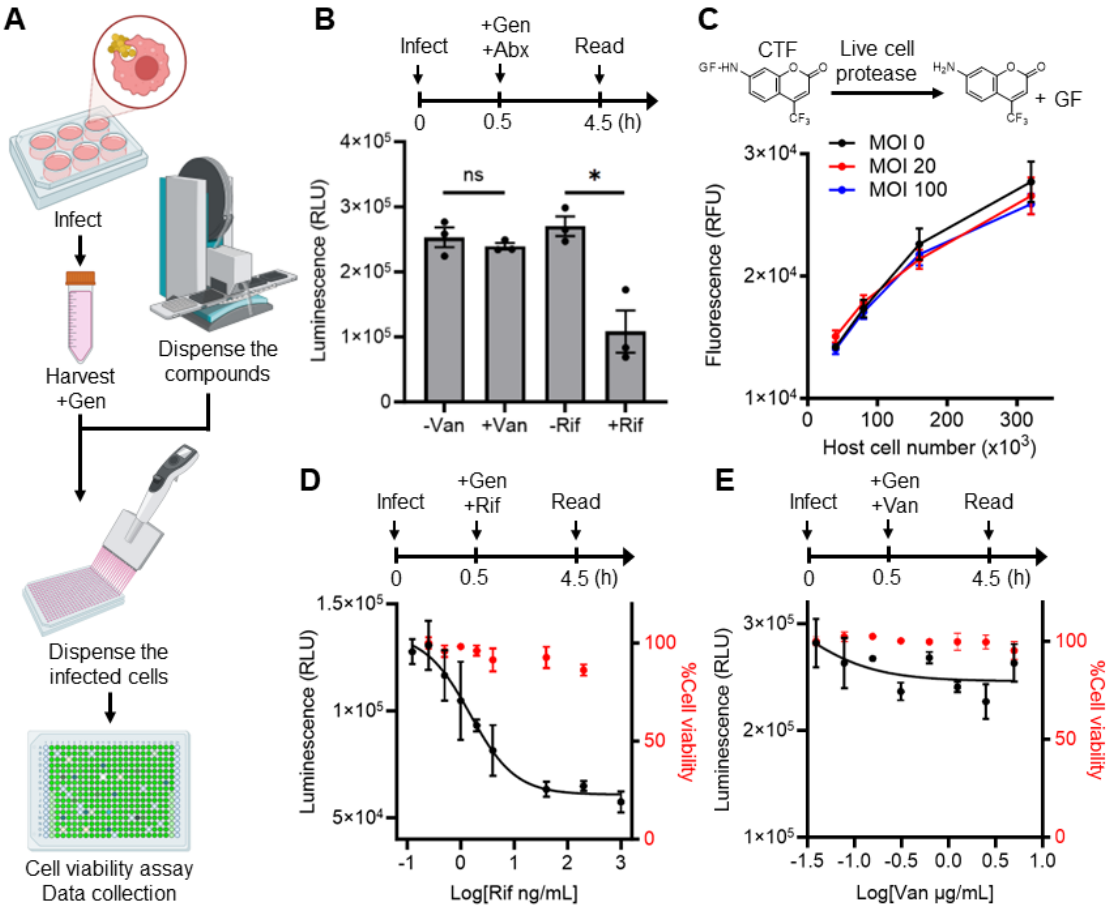

Figure 2. An established high-throughput screen allows for identifying compounds that modulate the energy state of intracellular *S. aureus*. (**A**) Schematic representation of the constructed compound screen for energy modulators of the intracellular bacteria. (**B**) The intracellular *S. aureus* activity can be probed using a bioluminescent MRSA strain JE2–lux. RAW 264.7 macrophages were infected with JE2–lux and treated with 20 µg/mL vancomycin (Van) or 10 µg/mL rifampicin (Rif) for 4 h before luminescence detection. Gentamicin (Gen; 50 µg/mL) was also added to eliminate the extracellular bacteria. Only Rif can penetrate the host plasma membrane and target the intracellular bacteria. Representative data of three biological replicates is shown (n = 3). *p<0.05; ns, not significant (unpaired t-test). The bars represent mean ± SEM. (**C**) The

638 host cell viability can be monitored using CellTiter-Fluor (CTF). The enzymatic reaction
639 reflected the number of viable RAW 264.7 cells (Pearson correlation coefficient $r > 0.97$,
640 $p < 0.05$) and was not interfered with the presence of *S. aureus*. The multiplicities of
641 infection (MOIs) of 0 (black), 20 (red) and 100 (blue) are shown (n = 3). (**D** and **E**) Dose
642 response curves for Rif (**D**) and Van (**E**) inhibition of intracellular *S. aureus* activity (black
643 circles). The host cell viability was simultaneously measured (red circles). Representative
644 data of three biological replicates is shown (n = 3). The bars represent mean ± SEM.
645 Assay schematics are shown above plots.
646
647

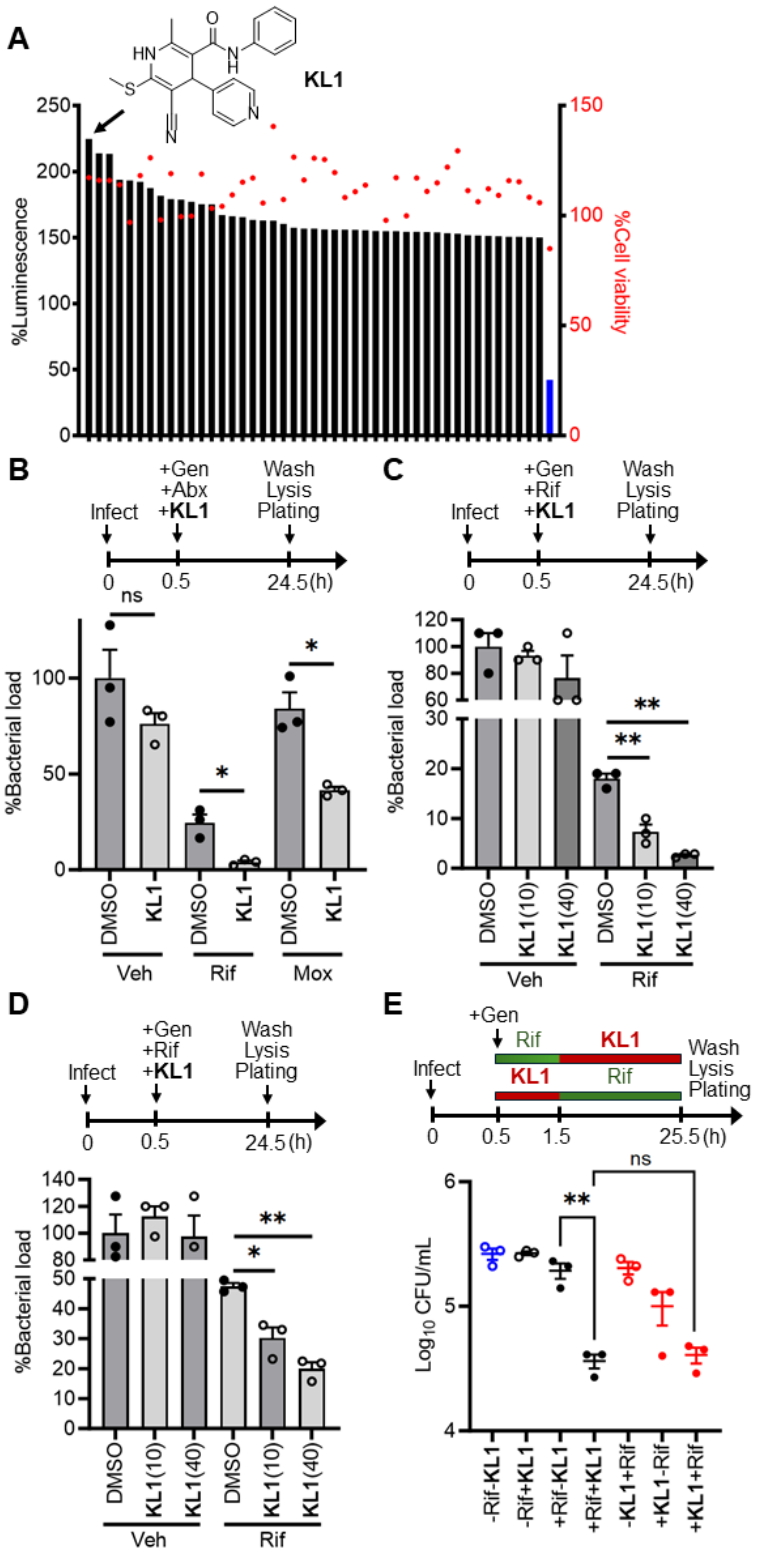

648

649 **Figure 3. Screening a kinase-targeted compound library identifies a small molecule**

650 **that sensitizes intracellular *S. aureus* to antibiotic killing.** (**A**) Forty-five compounds

651 (10 μM) exhibited >1.5-fold increase in the luminescence signal (black bars) comparing
652 to the vehicle control (0.1% DMSO). No cytotoxicity was observed in the 4-h treatment
653 window (red circles). The chemical structure of the top candidate compound **KL1** is shown.
654 The rifampicin-treated group was included as a reference (blue bar). (**B**) **KL1** (open
655 circles) facilitates rifampicin (Rif; 10 μg/mL) and moxifloxacin (Mox; 50 μg/mL) killing of
656 the intracellular MRSA. Gentamicin (Gen; 50 μg/mL) was added to eradicate the
657 extracellular bacteria. The numbers of survivor bacteria were normalized to the untreated
658 control (no antibiotics (Abx), no **KL1**, Gen-only) (n = 3). (**C** and **D**) The **KL1**-mediated
659 synergism was detected in different clinical isolates with the high persister (**C**) and low
660 persister (**D**) phenotypes characterized in Figure 1A. A dose-dependent sensitization was
661 observed with 0–40 μM **KL1** in these isolates (n = 3). (**E**) Pre-exposure to Abx does not
662 affect the sensitization by **KL1**. Infected RAW 264.7 cells were treated with either 10
663 μg/mL Rif (black circles) or 40 μM **KL1** (red circles) for 1 h, followed by the addition of
664 **KL1** and Rif, respectively. The untreated group (blue circles) was included as a negative
665 control (n = 3). Assay schematic above plot indicates the orders of the treatment regimens.
666 *p<0.05; **p<0.01; ns, not significant (unpaired t-test). The bars represent mean ± SEM.
667
668
669
670

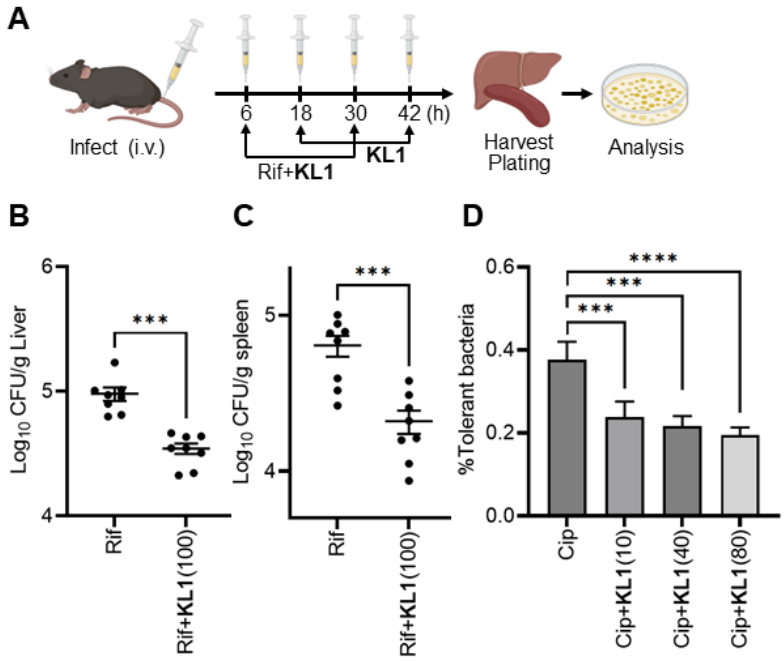

Figure 4. The identified compound KL1 enhances antibiotic killing of *S. aureus* in a murine bacteremia model and *Salmonella Typhimurium* in macrophages. (**A**) Schematic representation of the murine model. C57BL/6J mice were infected via intravenous (i.v.) tail vein injections and intraperitoneally treated with 10 mg/kg rifampicin (Rif) (q.d.) with and without 100 mg/kg **KL1** (b.i.d.) at 6 hours post-infection (hpi) for 2 days. The organs were harvested and homogenized to enumerate the numbers of survivor bacteria (CFU). Co-administration of **KL1** and Rif reduced the bacterial burden in the liver (**B**) and spleen (**C**). Representative data of two independent experiments was shown (n = 8). A total of 14 mice per treatment group were examined. ***p<0.001 (unpaired t-test). (**D**) **KL1** facilitates ciprofloxacin (Cip; 5 μg/mL) killing of intracellular *Salmonella Typhimurium*. The numbers of survivor bacteria were normalized to the input CFUs (T_0) (n = 7–8). ***p<0.001; ****p<0.0001 (two-way ANOVA). The bars represent mean ± SEM.

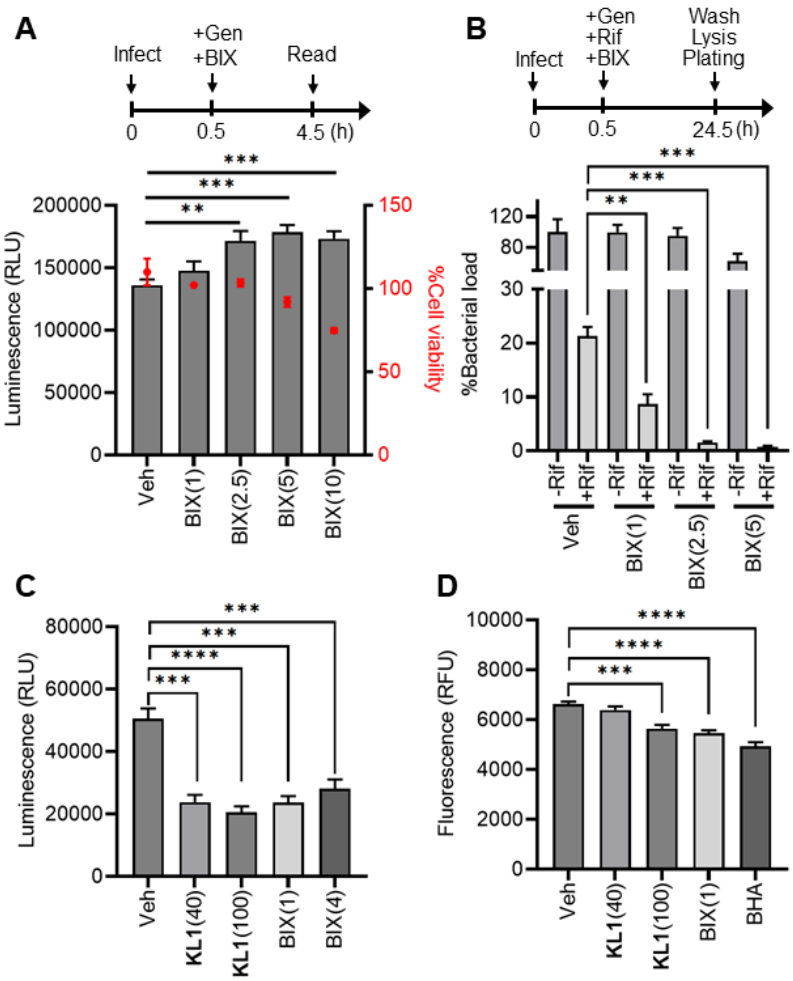

686

687 **Figure 5. KL1 reduces the production of reactive oxygen species upon infection.**
688 (**A**) Inhibition of G9a/EHMT2 phenocopies the **KL1**-mediated sensitization in intracellular
689 *S. aureus*. A selective G9a inhibitor, BIX-01294 (BIX; 2.5–10 μM), increased the
690 bioluminescence signal (grey bars) of strain JE2–lux comparing to the vehicle control
691 (Veh, 0.1% DMSO). The relative cytotoxicity of BIX was examined (red circles).
692 Representative data of three independent experiments is shown (n = 5). (**B**) The G9a
693 inhibitor increases rifampicin (Rif; 10 μg/mL) killing of the intracellular MRSA in a dose-
694 dependent manner (1–5 μM). Gentamicin (Gen; 50 μg/mL) was added to eradicate the
695 extracellular bacteria. The numbers of survivor bacteria were normalized to the untreated
696 control (no Rif, no BIX, Gen-only) (n = 3). Both **KL1** (40 and 100 μM) and BIX (1 and 4

697 μM) reduce ROS production at 4 hours post-infection (hpi). A chemiluminescent probe L-
698 012 (**C**) and a fluorescent probe fluorescein-boronate (Fl-B) (**D**) were utilized to quantify
699 reactive species in infected macrophages. An antioxidant butylated hydroxyanisole (BHA;
700 20 μM) was included as a control. Representative data of three independent experiments
701 are shown (n = 5). Assay schematics are shown above plots. **$p<0.01$; ***$p<0.001$;
702 ****$p<0.0001$ (unpaired t-test). The bars represent mean ± SEM.
703
704

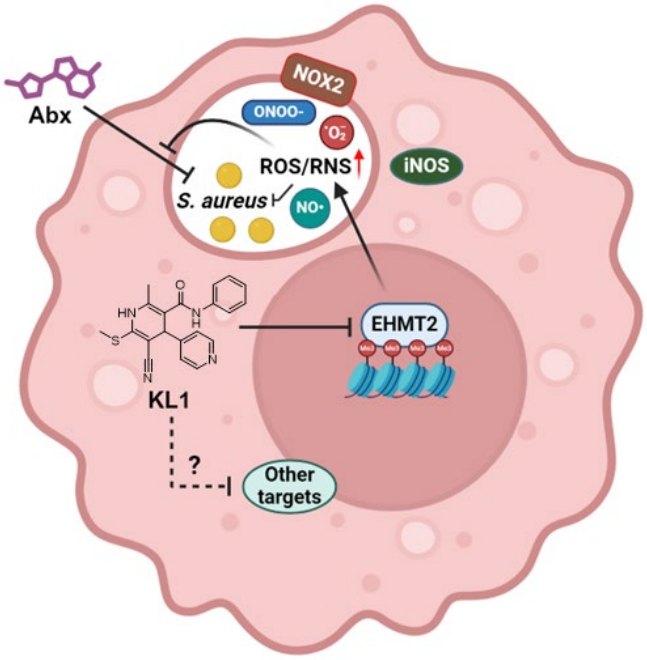

705

706 **Figure 6. Mechanistic model of KL1-mediated sensitization of intracellular *S.***
707 ***aureus*.** Host-derived reactive oxygen and nitrogen species (ROS/RNS) help contain
708 intracellular *S. aureus* infections but also antagonize antibiotics by collapsing the bacterial
709 metabolism and forcing the bacteria into antibiotic-tolerant persister cells. The identified
710 compound **KL1** sensitizes intracellular bacteria to antibiotic killing by reducing the
711 production of reactive species upon infection, presumably by targeting the G9a/EHMT2
712 activity.

713

714 **Supplementary table 1. Minimum inhibitory concentrations (MICs) of antibiotics in**

715 **the *S. aureus* strains used in this study.**

Antibiotics	LAC	JE2–Lux	High persister	Low persister
Rifampicin	0.008±0.004 μg/mL	0.006 μg/mL	0.006 μg/mL	0.008±0.004 μg/mL
Moxifloxacin	5 μg/mL	5 μg/mL	0.16 μg/mL	0.16 μg/mL
Vancomycin	1.33±0.58 μg/mL	1 μg/mL	1.33±0.58 μg/mL	1 μg/mL

716 Three independent experiments were conducted, and the MIC values are presented as

717 the average ± the standard deviation.

718

719

720

721

722 **Supplementary table 2. Potential targets of KL1 based on published functional**

723 **screens.**

Target	BioAssay ID†	Assay	Activity	Location, expression‡
PHOSPHO1	1565	uHTS absorbance assay for the identification of compounds that inhibit PHOSPHO1	61.5% inhibition at 13.3 μM	Intracellular, immune cells and other cell types
SLC5A7	488975	Primary cell-based screen for identification of compounds that inhibit the Choline Transporter	BScore_intRatio of -5.0281	Membrane, not detected in immune cells
SLC5A7	493221	Confirmatory screen for compounds that inhibit the Choline Transporter	50.55% inhibition at 10 μM	Membrane, not detected in immune cells
EHMT2/G9a	504332	qHTS Assay for Inhibitors of Histone Lysine Methyltransferase G9a	EC_{50} value of 25.12 μM	Intracellular, immune cells and other cell types
COPS5	651999	uHTS identification of small molecule inhibitors of Csn-mediated Deneddylation of Cullin-Ring Ligases, vis a fluorescence polarization assay	93.48% inhibition at 12.5 μM	Intracellular, immune cells and other cell types

724 †Data sourced form PubChem biological test results.

725 ‡Data sourced form Expression Atlas.

726

727

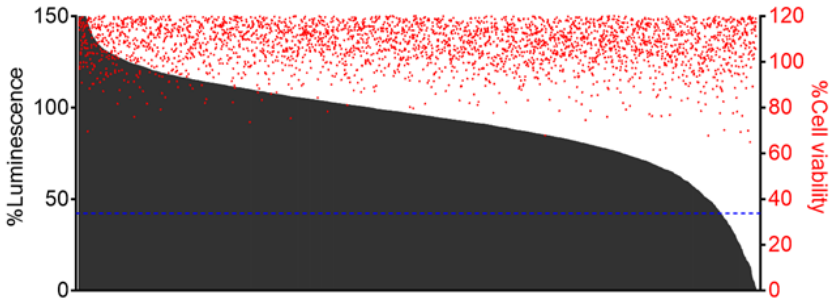

728

729 **Supplementary figure 1. High-throughput screening of a kinase-targeted library**
730 **identifies compounds with differential capacities in modulating the energy state of**
731 **intracellular *S. aureus*.** A total of >4,700 compounds (10 μM) from the UNC CICBDD
732 were screened for targeting the intracellular MRSA. All of these compounds shared
733 structural similarity to kinase inhibitors and complied with the Lipinski's rule of five. The
734 luminescence signals were normalized to the vehicle controls (0.1% DMSO) (black bars).
735 The normalized host cell viability was measured by the CellTiter-Fluor assay (red circles).
736 The %luminescence of 10 μg/mL rifampicin-treated cells is indicated as a reference (blue
737 dashed line).

738

739

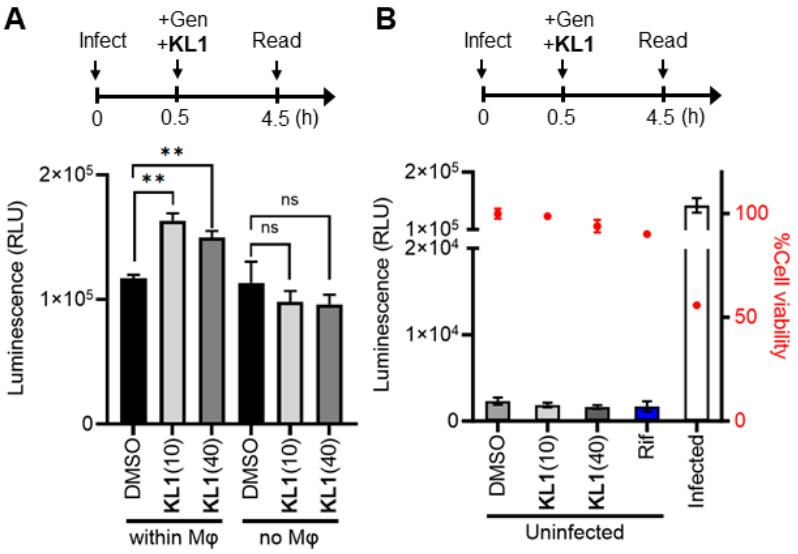

Supplementary figure 2. The energy state up-regulation by KL1 is not caused by background noises from the compound, the host cells or the dead extracellular bacteria. (**A**) Macrophages infected with the bioluminescent MRSA strain JE2–lux (within Mφ) were treated with 10 μM or 40 μM **KL1**. Gentamicin (Gen; 50 μg/mL) was added to eliminate the extracellular bacteria. The bacterial cultures without macrophages (no Mφ) in the presence of Gen were examined with the same input CFU and culture conditions (n = 3). (**B**) Uninfected macrophages were treated with 10 μM or 40 μM **KL1**. The normalized host cell viability was measured by the CellTiter-Fluor assay (red circles). Rifampicin (Rif)-treated cells (blue bar) and infected macrophages (white bar) were included as controls (n = 3). Assay schematics are shown above plots. **$p<0.01$; ns, not significant (unpaired t-test). The bars represent mean ± SEM.

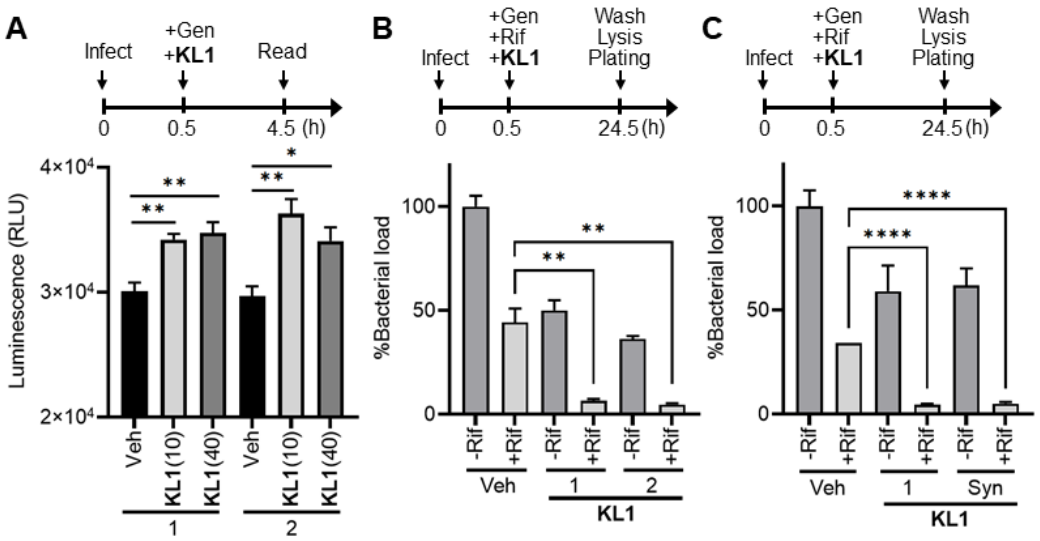

755

756 **Supplementary figure 3. The adjuvant activity of KL1 was consistently observed**
757 **with the compound across different sources.** (**A** and **B**) **KL1** (10 and 40 μM)
758 purchased from two independent suppliers, ChemBridge (1) and Enamine (2),
759 consistently elevated the energy state of intracellular *S. aureus* (n = 4) and sensitized the
760 bacteria to killing by rifampicin (Rif, 10 μg/mL) (n = 3). (**C**) **KL1** synthesized in-house (Syn)
761 displayed adjuvant activity comparable to that of commercially available **KL1** (n = 3).
762 Gentamicin (Gen; 50 μg/mL) was added to eradicate the extracellular bacteria. The
763 numbers of tolerant bacteria were normalized to the untreated control (no Rif, no BIX,
764 Gen-only). Assay schematics are shown above plots. *p<0.05; **p<0.01; ****p<0.0001
765 (unpaired t-test). The bars represent mean ± SEM.

766

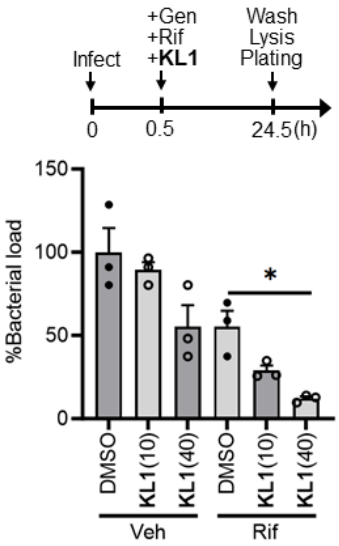

767

768 **Supplementary figure 4. Compound KL1 sensitizes the killing of intracellular MRSA**

769 **by antibiotics in a dose-dependent manner.** RAW 264.7 cells were infected with the

770 MRSA strain JE2–lux and treated with 10 μM or 40 μM **KL1** in the presence or absence

771 of 10 μg/mL rifampicin (Rif). Gentamicin (Gen; 50 μg/mL) was added to eliminate the

772 extracellular bacteria. The numbers of survivor bacteria were normalized to the untreated

773 control (no Rif, no **KL1**, Gen-only) (n = 3). *$p<0.05$ (unpaired t-test). The bars represent

774 mean ± SEM.

775

776

777

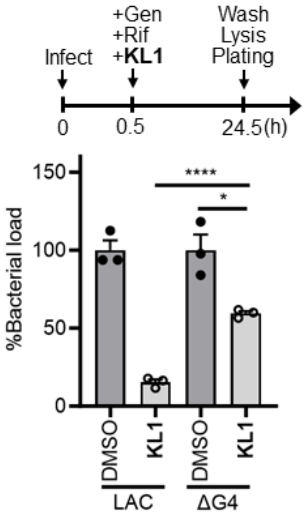

Supplementary figure 5. Glucose uptake is important for the synergism between KL1 and antibiotics. RAW 264.7 cells were infected with the wild-type strain LAC or the mutant lacking all four glucose transporters (ΔG4). The infected cells were treated with 40 μM **KL1** and 10 μg/mL rifampicin (Rif). Gentamicin (Gen) was included to eliminate the extracellular bacteria. The numbers of survivor bacteria were normalized to the corresponding controls (no **KL1**, Gen- and Rif-only) (black circles) (n = 3). *$p<0.05$; ****$p<0.0001$ (unpaired t-test). The bars represent mean ± SEM.

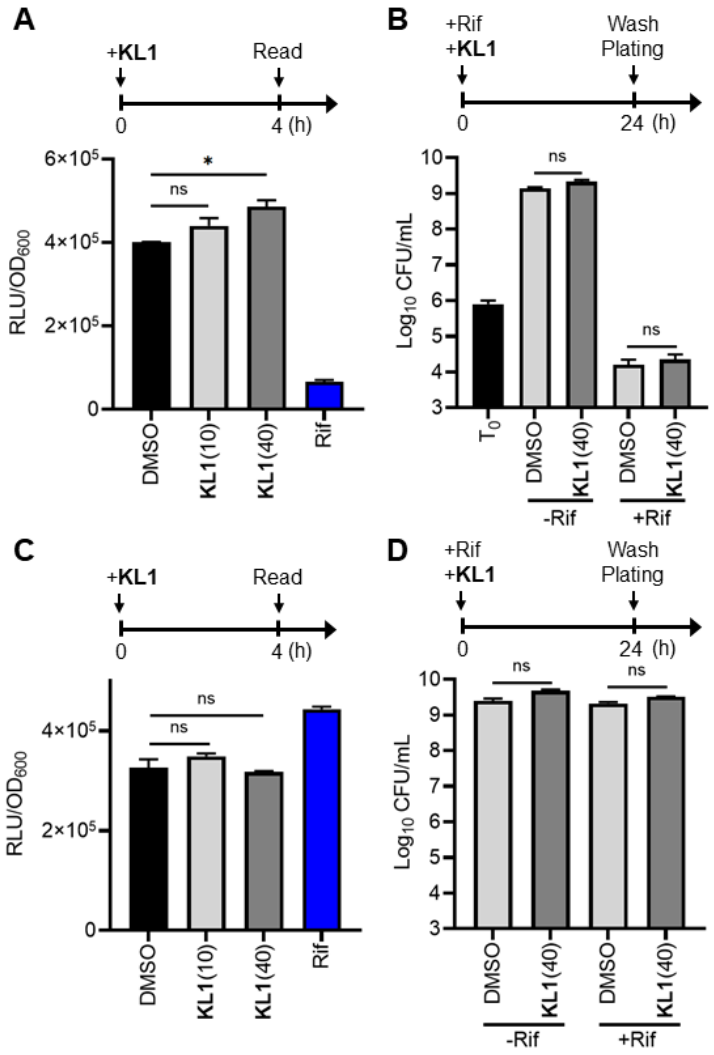

Supplementary figure 6. Compound KL1 exhibits a minute effect on the extracellular *S. aureus* activity and does not synergize with antibiotics in killing the extracellular bacteria. (**A** and **C**) The exponential-phase (**A**) and stationary-phase (**C**) *S. aureus* cultures (JE2–lux) were incubated with 10 μM or 40 μM **KL1** for 4 h, followed by luminescence detection. The signal intensities (RLU) were normalized to the OD_{600} values. The vehicle control (0.1% DMSO, black bar) and rifampicin (Rif; 2 μg/mL)-treated group (blue bar) were included as references. (**B** and **D**) The exponential-phase (**B**) and stationary-phase (**D**) cultures were treated with and without 40 μM **KL1** and 2 μg/mL Rif

796 for 24 h, followed by a wash step and plating to enumerate the number of tolerant bacteria.

797 Assay schematics are shown above plots. *$p<0.05$; ns, not significant (unpaired t-test).

798 The bars represent mean ± SEM.

799

800

801

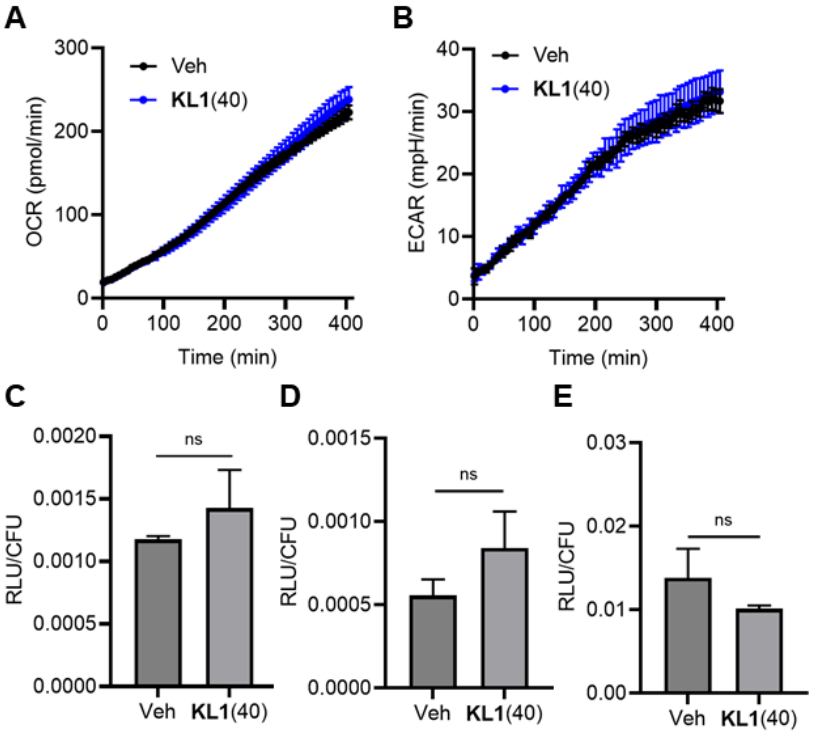

802

803 **Supplementary figure 7. Compound KL1 does not impact the metabolic activity and**
804 **ATP levels in extracellular bacteria.** (**A** and **B**) Metabolic analysis indicates that **KL1**
805 (40 μM, blue) does not alter the oxygen consumption rate (OCR) (**A**) and extracellular
806 acidification rate (ECAR) (**B**) in extracellular *S. aureus* comparing to the vehicle control
807 (Veh, 0.1–0.5% DMSO, black). Representative data of six independent experiments (n =
808 3) is shown. The bars represent mean ± SD. (**C**–**E**) Exponential-phase cultures were
809 treated with 40 μM **KL1** or 0.1% DMSO for 4 h, followed by measuring the relative ATP
810 levels using a BacTiter-Glo assay. The luminescent signals were normalized to the
811 numbers of bacteria. *S. aureus* strains HG003 (**C**), JE2 (**D**) and LAC (**E**) were examined
812 (n = 3–6). ns, not significant (unpaired t-test).

813

814

815

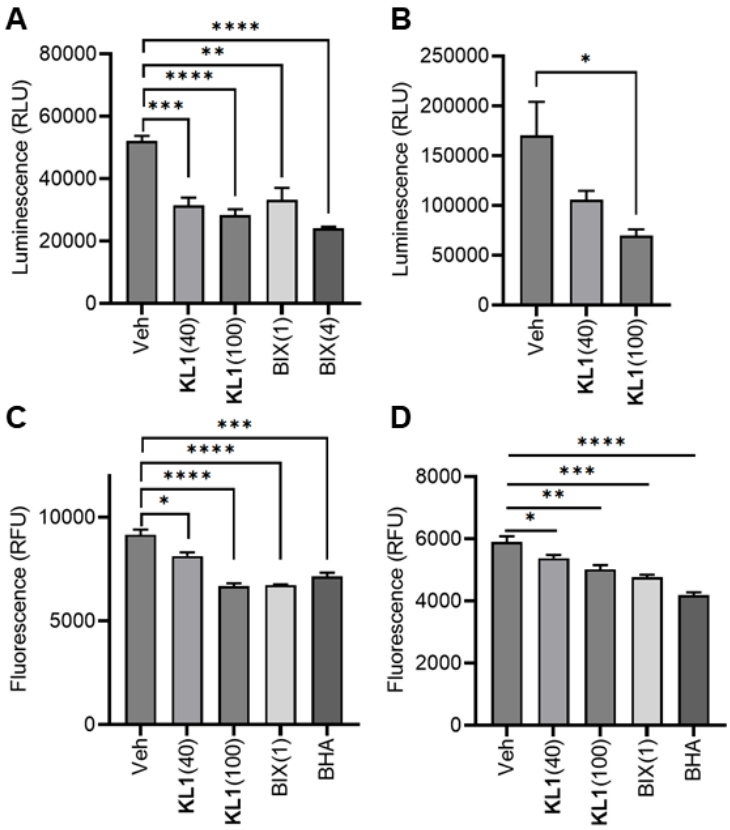

816

817 **Supplementary figure 8. KL1 reduces the level of reactive oxygen species in both**
818 **infected and uninfected macrophages.** Compound **KL1** (40 and 100 μM) and the G9a
819 inhibitor, BIX-01294 (BIX; 1 and 4 μM) decreased the ROS level in *S. aureus*-infected
820 macrophages at 8 hours post-infection (hpi) (**A** and **C**) and in uninfected macrophages (**B**
821 and **D**). L-012 (**A** and **B**) and fluorescein-boronate (Fl-B) (**C** and **D**) were used to quantify
822 the ROS level. DMSO (Veh; 0.25%) and butylated hydroxyanisole (BHA; 20 μM) was
823 included as controls. Representative data of three independent experiments are shown
824 (n = 5). *p<0.05; **p<0.01; ***p<0.001; ****p<0.0001 (unpaired t-test). The bars represent
825 mean ± SEM.

826

827

828 ## References

829 1. M. Huemer *et al.*, Molecular reprogramming and phenotype switching in
830 Staphylococcus aureus lead to high antibiotic persistence and affect therapy
831 success. *Proc Natl Acad Sci U S A* **118** (2021).
832 2. N. D. Hicks *et al.*, Clinically prevalent mutations in Mycobacterium tuberculosis
833 alter propionate metabolism and mediate multidrug tolerance. *Nat Microbiol* **3**,
834 1032-1042 (2018).
835 3. R. A. Fisher, B. Gollan, S. Helaine, Persistent bacterial infections and persister
836 cells. *Nat Rev Microbiol* **15**, 453-464 (2017).
837 4. L. F. Westblade, J. Errington, T. Dorr, Antibiotic tolerance. *PLoS Pathog* **16**,
838 e1008892 (2020).
839 5. N. Q. Balaban *et al.*, Definitions and guidelines for research on antibiotic
840 persistence. *Nat Rev Microbiol* **17**, 441-448 (2019).
841 6. K. Y. Lu *et al.*, Antibiotic Tolerance and Treatment Outcomes in Cystic Fibrosis
842 Methicillin-Resistant Staphylococcus aureus Infections. *Microbiol Spectr* **11**,
843 e0406122 (2023).
844 7. R. Kuehl, L. Morata, S. Meylan, J. Mensa, A. Soriano, When antibiotics fail: a
845 clinical and microbiological perspective on antibiotic tolerance and persistence of
846 Staphylococcus aureus. *J Antimicrob Chemother* **75**, 1071-1086 (2020).
847 8. I. Levin-Reisman *et al.*, Antibiotic tolerance facilitates the evolution of resistance.
848 *Science* **355**, 826-830 (2017).
849 9. I. Santi, P. Manfredi, E. Maffei, A. Egli, U. Jenal, Evolution of Antibiotic Tolerance
850 Shapes Resistance Development in Chronic Pseudomonas aeruginosa Infections.
851 *mBio* **12** (2021).

852 10. B. P. Conlon *et al.*, Persister formation in Staphylococcus aureus is associated with
853 ATP depletion. *Nat Microbiol* **1** (2016).
854 11. M. L. Pinel-Marie *et al.*, RNA antitoxin SprF1 binds ribosomes to attenuate
855 translation and promote persister cell formation in Staphylococcus aureus. *Nat*
856 *Microbiol* **6**, 209-220 (2021).
857 12. J. A. Freiberg *et al.*, Restriction of arginine induces antibiotic tolerance in
858 Staphylococcus aureus. *Nat Commun* **15**, 6734 (2024).
859 13. S. E. Rowe *et al.*, Reactive oxygen species induce antibiotic tolerance during
860 systemic Staphylococcus aureus infection. *Nat Microbiol* **5**, 282-290 (2020).
861 14. J. E. Beam *et al.*, Macrophage-Produced Peroxynitrite Induces Antibiotic Tolerance
862 and Supersedes Intrinsic Mechanisms of Persister Formation. *Infect Immun* **89**,
863 e0028621 (2021).
864 15. F. Peyrusson *et al.*, Intracellular Staphylococcus aureus persisters upon antibiotic
865 exposure. *Nat Commun* **11**, 2200 (2020).
866 16. S. Helaine *et al.*, Internalization of Salmonella by macrophages induces formation
867 of nonreplicating persisters. *Science* **343**, 204-208 (2014).
868 17. Y. Liu *et al.*, Immune activation of the host cell induces drug tolerance in
869 Mycobacterium tuberculosis both in vitro and in vivo. *J Exp Med* **213**, 809-825
870 (2016).
871 18. S. Helaine, B. P. Conlon, K. M. Davis, D. G. Russell, Host stress drives tolerance
872 and persistence: The bane of anti-microbial therapeutics. *Cell Host Microbe* **32**,
873 852-862 (2024).
874 19. F. Peyrusson, T. K. Nguyen, T. Najdovski, F. Van Bambeke, Host Cell Oxidative
875 Stress Induces Dormant Staphylococcus aureus Persisters. *Microbiol Spectr* **10**,

876 e0231321 (2022).
877 20. J. R. Raneses, A. L. Ellison, B. Liu, K. M. Davis, Subpopulations of Stressed
878 Yersinia pseudotuberculosis Preferentially Survive Doxycycline Treatment within
879 Host Tissues. *mBio* **11** (2020).
880 21. P. W. S. Hill *et al.*, The vulnerable versatility of Salmonella antibiotic persisters
881 during infection. *Cell Host Microbe* **29**, 1757-1773 e1710 (2021).
882 22. B. G. Surewaard *et al.*, Identification and treatment of the Staphylococcus aureus
883 reservoir in vivo. *J Exp Med* **213**, 1141-1151 (2016).
884 23. P. Sendi, R. A. Proctor, Staphylococcus aureus as an intracellular pathogen: the
885 role of small colony variants. *Trends Microbiol* **17**, 54-58 (2009).
886 24. S. Clement *et al.*, Evidence of an intracellular reservoir in the nasal mucosa of
887 patients with recurrent Staphylococcus aureus rhinosinusitis. *J Infect Dis* **192**,
888 1023-1028 (2005).
889 25. R. S. Flannagan, B. Heit, D. E. Heinrichs, Intracellular replication of
890 Staphylococcus aureus in mature phagolysosomes in macrophages precedes host
891 cell death, and bacterial escape and dissemination. *Cell Microbiol* **18**, 514-535
892 (2016).
893 26. C. Garzoni, W. L. Kelley, Staphylococcus aureus: new evidence for intracellular
894 persistence. *Trends Microbiol* **17**, 59-65 (2009).
895 27. P. Nandhini *et al.*, Recent Developments in Methicillin-Resistant Staphylococcus
896 aureus (MRSA) Treatment: A Review. *Antibiotics (Basel)* **11** (2022).
897 28. P. Santucci *et al.*, Intracellular localisation of Mycobacterium tuberculosis affects
898 efficacy of the antibiotic pyrazinamide. *Nat Commun* **12**, 3816 (2021).
899 29. S. Ronneau, C. Michaux, R. T. Giorgio, S. Helaine, Intoxication of antibiotic

900 persisters by host RNS inactivates their efflux machinery during infection. *PLoS*
901 *Pathog* **20**, e1012033 (2024).
902 30. P. Hovhannisyan *et al.*, Infection of human organoids supports an intestinal niche
903 for Chlamydia trachomatis. *PLoS Pathog* **20**, e1012144 (2024).
904 31. H. Liu *et al.*, Staphylococcus aureus Epicutaneous Exposure Drives Skin
905 Inflammation via IL-36-Mediated T Cell Responses. *Cell Host Microbe* **22**, 653-666
906 e655 (2017).
907 32. L. R. Thurlow, A. C. Stephens, K. E. Hurley, A. R. Richardson, Lack of nutritional
908 immunity in diabetic skin infections promotes Staphylococcus aureus virulence.
909 *Sci Adv* **6** (2020).
910 33. M. A. Lobritz *et al.*, Antibiotic efficacy is linked to bacterial cellular respiration. *Proc*
911 *Natl Acad Sci U S A* **112**, 8173-8180 (2015).
912 34. Y. Li, G. Li, L. Zhang, Y. Li, Z. Zhao, G9a promotes inflammation in Streptococcus
913 pneumoniae induced pneumonia mice by stimulating M1 macrophage polarization
914 and H3K9me2 methylation in FOXP1 promoter region. *Ann Transl Med* **10**, 583
915 (2022).
916 35. A. Muneer *et al.*, Non-canonical function of histone methyltransferase G9a in the
917 translational regulation of chronic inflammation. *Cell Chem Biol* **30**, 1525-1541
918 e1527 (2023).
919 36. X. Wang *et al.*, Histone methyltransferases G9a mediated lipid-induced M1
920 macrophage polarization through negatively regulating CD36. *Metabolism* **114**,
921 154404 (2021).
922 37. K. L. Cotten, K. M. Davis, Bacterial heterogeneity and antibiotic persistence:
923 bacterial mechanisms utilized in the host environment. *Microbiol Mol Biol Rev* **87**,

924 e0017422 (2023).
925 38. C. Liu *et al.*, Clinical practice guidelines by the infectious diseases society of
926 america for the treatment of methicillin-resistant Staphylococcus aureus infections
927 in adults and children. *Clin Infect Dis* **52**, e18-55 (2011).
928 39. A. D. Bai *et al.*, Staphylococcus aureus bacteraemia mortality: a systematic review
929 and meta-analysis. *Clin Microbiol Infect* **28**, 1076-1084 (2022).
930 40. J. Tasse, G. Dieppois, F. Peyrane, N. Tesse, Improving the ability of antimicrobial
931 susceptibility tests to predict clinical outcome accurately: Adding metabolic evasion
932 to the equation. *Drug Discov Today* **26**, 2182-2189 (2021).
933 41. H. Niu, J. Gu, Y. Zhang, Bacterial persisters: molecular mechanisms and
934 therapeutic development. *Signal Transduct Target Ther* **9**, 174 (2024).
935 42. B. Gollan, G. Grabe, C. Michaux, S. Helaine, Bacterial Persisters and Infection:
936 Past, Present, and Progressing. *Annu Rev Microbiol* **73**, 359-385 (2019).
937 43. A. Harms, E. Maisonneuve, K. Gerdes, Mechanisms of bacterial persistence
938 during stress and antibiotic exposure. *Science* **354** (2016).
939 44. D. D. Rockey, X. Wang, A. Debrine, N. Grieshaber, S. S. Grieshaber, Metabolic
940 dormancy in Chlamydia trachomatis treated with different antibiotics. *Infect Immun*
941 **92**, e0033923 (2024).
942 45. I. Keren, S. Minami, E. Rubin, K. Lewis, Characterization and transcriptome
943 analysis of Mycobacterium tuberculosis persisters. *mBio* **2**, e00100-00111 (2011).
944 46. C. H. Luk *et al.*, Salmonella enters a dormant state within human epithelial cells
945 for persistent infection. *PLoS Pathog* **17**, e1009550 (2021).
946 47. W. Eisenreich, T. Rudel, J. Heesemann, W. Goebel, Persistence of Intracellular
947 Bacterial Pathogens-With a Focus on the Metabolic Perspective. *Front Cell Infect*

948 *Microbiol* **10**, 615450 (2020).
949 48. J. E. Beam *et al.*, Inflammasome-mediated glucose limitation induces antibiotic
950 tolerance in Staphylococcus aureus. *iScience* **26**, 107942 (2023).
951 49. E. Blasi *et al.*, Selective immortalization of murine macrophages from fresh bone
952 marrow by a raf/myc recombinant murine retrovirus. *Nature* **318**, 667-670 (1985).
953 50. B. T. Bateman, N. P. Donegan, T. M. Jarry, M. Palma, A. L. Cheung, Evaluation of
954 a tetracycline-inducible promoter in Staphylococcus aureus in vitro and in vivo and
955 its application in demonstrating the role of sigB in microcolony formation. *Infect*
956 *Immun* **69**, 7851-7857 (2001).
957 51. M. R. Grosser, A. R. Richardson, Method for Preparation and Electroporation of S.
958 aureus and S. epidermidis. *Methods Mol Biol* **1373**, 51-57 (2016).
959 52. N. W. de Jong, T. van der Horst, J. A. van Strijp, R. Nijland, Fluorescent reporters
960 for markerless genomic integration in Staphylococcus aureus. *Sci Rep* **7**, 43889
961 (2017).
962 53. R. M. Corrigan, T. J. Foster, An improved tetracycline-inducible expression vector
963 for Staphylococcus aureus. *Plasmid* **61**, 126-129 (2009).
964 54. J. Schindelin *et al.*, Fiji: an open-source platform for biological-image analysis. *Nat*
965 *Methods* **9**, 676-682 (2012).
966 55. R. Nistala, A. Meuth, C. Smith, A. Annayya, Reliable and High Efficiency Extraction
967 of Kidney Immune Cells. *J Vis Exp* 10.3791/54368 (2016).
968 56. S. Kim *et al.*, PubChem 2023 update. *Nucleic Acids Res* **51**, D1373-D1380 (2023).
969 57. I. Papatheodorou *et al.*, Expression Atlas: gene and protein expression across
970 multiple studies and organisms. *Nucleic Acids Res* **46**, D246-D251 (2018).
971 58. C. UniProt, UniProt: the Universal Protein Knowledgebase in 2023. *Nucleic Acids*

Res **51**, D523-D531 (2023).